A ONE-DIMENSIONAL RADIATIVE-CONVECTIVE MODEL OF THE EARTH'S ATMOSPHERE FOR CLIMATE APPLICATIONS

Wei-chyung Wang and Andrew A. Lacis

NASA, Goddard Institute for Space Studies
Goddard Space Flight Center
New York, New York 10025

(NASA-TM-103084) A ONE-DIMENSIONAL RADIATIVE-CONVECTIVE MODEL OF THE EARTH'S ATMOSPHERE FOR CLIMATE APPLICATIONS (NASA) 58 p

N90-71349

Unclas
00/45 0277465

ABSTRACT

This paper describes a one-dimensional time dependent radiative-convective model for the earth's atmosphere. The model includes the radiative effects of clouds, aerosols, the major radiative gases (H_2O, CO_2, O_3) and minor gaseous constituents. A simple convective adjustment process is used to parameterize the vertical transport of heat by atmospheric motions.

Solar radiative transfer is computed with the doubling and adding method. For terrestrial radiation we use approximate analytic solutions for a single layer and then the adding method to compute fluxes at the layer interfaces. Multiple scattering is explicitly modeled for both solar and terrestrial radiation. Integration over frequency including the effects of atmospheric inhomogeneity, i.e., pressure and temperature change with altitude, is accurately handled for both solar and terrestrial radiation by use of a generalization of the k-distribution method.

The sensitivity of atmospheric thermal structure to assumptions about the critical lapse rate for convective adjustment, cloud parameters and atmospheric humidity is studied. It is shown that the critical lapse rate is crucial for determining the surface temperature change in climate perturbations. For example, if the abundance of atmospheric CO_2 is doubled the computed surface temperature is increased by 2.0K for a fixed lapse rate of 6.5 K km^{-1}, but by only 1.4 K for the moist-adiabatic lapse rate. We also show that cloud base altitudes have as large an effect as the cloud top altitudes on the computed surface temperature.

As a sample application we compute the change in the atmospheric temperature profile which would result from ozone profile predicted on the

assumption of an order of magnitude increase in atmospheric chlorofluoromethanes; the ozone perturbation amounts to an decrease of 18 percent in the column abundance with a maximum decrease of 50 percent at 40 km altitude. The ozone reduction leads to a 0.2 K cooling of the troposphere and surface which is overwhelmed by the greenhouse warming of the added chlorofluoromethanes. The net result is a warming of about 0.1 K.

1. Introduction

One-dimensional radiative-convective models which determine the thermal structure of the atmosphere as a result of the balance between radiative flux and a parameterized convective flux are useful tools for climate studies (cf. Schneider and Dickinson 1974 for climate modeling). These models, which can include realistic vertical distributions of radiatively-important atmospheric constituents, can be used to examine the role that these constituents play in determining the global mean temperature structure (e.g. Manabe and Wetherald, 1967; Wang and Domoto, 1974; Ramanathan, 1975, 1976a,b; Wang et al., 1976; Hansen et al., 1978). Although such models exclude a number of major feedback mechanisms, it is conceivable that the model provides good estimates for the first order radiative effect of a perturbation of atmospheric constituents.

For climate studies, it is essential to have a rapid and accurate method for computation of radiative heatings and coolings which provide the radiative temperature changes. Furthermore, besides radiative fluxes other processes, such as vertical convection (evaluated according to assigned critical lapse rate), cloudiness and humidity are parameterized one-dimensionally. Consequently the model results will be affected by the accuracy of radiative model employed as well as the parameterizations used for other energy transfer processes. The present paper gives a detailed description of radiative calculations and examines the sensitivity of computed results to model parameters inherited in the one-dimensional radiative-convective model.

2. Radiative transfer calculation

The basic problem encountered in the calculations of radiative transfer in a realistic atmosphere is the inseparable processes of scattering and absorption due to cloud and aerosol particles, and of absorption by atmospheric gases (Goody, 1964). The main difficulty is that the integration over frequency is not properly accounted for by the usual band model techniques for gaseous absorption which do not allow for multiple scattering, and direct line-by-line integration is too time consuming for practical use. We handle the frequency integration with the correlated k-distribution method described in Lacis et al. (1979). In this section, we first present the formulation for computing the monochromatic flux and next we briefly describe the method for using correlated k-distribution function.

a. Monochromatic flux calculation

The doubling and adding method is used for computing solar radiation. Detailed descriptions of the computational scheme used to calculate the solar intensities and fluxes can be found in Lacis and Hansen (1974). This method is further extended to include thermal emission in terrestrial radiation calculations. However, in order to avoid the time-consuming doubling method we have developed a more efficient way of computing terrestiral radiation. In this treatment, analytical expressions of emission, transmission and reflection function of single layer are obtained by solving the radiative transfer equation rather than using doubling method. Adding method is then employed for combining layers.

The radiative transfer equation for an emitting, scattering and absorbing layer is

$$\mu \frac{dI}{d\tau} = -I(\tau,\mu) + (1-\tilde{\omega}) I_b(\tau) + \frac{1}{2} \int_{-1}^{1} I(\tau,\mu') P_s(\tau,\mu,\mu') d\mu' \quad (1)$$

where $I(\tau,\mu)$ is the spectral intensity, θ the zenith angle ($\mu=\cos\theta$), τ the optical depth, $\tilde{\omega}$ the single scattering albedo ($\tilde{\omega} = k_s/k_t$ and $k_t = k_s + k_a$, with subscripts a, s and t denoting absorption, scattering and extinction respectively). I_b is the spectral Planck function. $P_s(\tau,\mu,\mu')$ is the scattering phase function; its first moment "g" characterizes the relative importance of forward-to-backward scattering (van de Hulst, 1963). The intensity is assumed to be independent of azimuthal angle (Chandrasekhar, 1960).

The boundary conditions for the isolated layer are

$$\begin{cases} I^+(0,\mu) = 0 \\ I^-(\tau_0,\mu) = 0 \end{cases} \tag{2}$$

where τ_0 is the optical thickness of the layer. One may note that I^+ corresponds to positive values of μ, where I^- is associated with negative μ values. Separate solutions for clear and cloudy layer are given below.

Clear Layer

For a layer without scatterers, the solutions can be written in integral form

$$\begin{cases} I^+(\tau,\mu) = \displaystyle\int_0^{\tau} I_b(x)\, e^{-(\tau-x)/\mu} d\left(\frac{x}{\mu}\right) \\ I^-(\tau,\mu) = -\displaystyle\int_{\tau}^{\tau_0} I_b(x)\, e^{-(\tau-x)/\mu} d\left(\frac{x}{\mu}\right) \end{cases} \tag{3}$$

For practical purpose a linear Planck function relation for the layer in assumed, i.e.,

$$\pi I_b(\tau) = B_b + m\tau \tag{4}$$

where $m = (B_t - B_b)/\tau_0$ and, B_b and B_t are the Planck functions at $\tau = 0$ and τ_0. This profile tends to overestimate the layer emissivity compared with the linear temperature relation. However, as indicated in a report by System, Science, and Software (1972), the approximation is very good for most atmospheric zones in most spectral regions. We have made further calculations inside the 10 μm atmospheric window with various temperature gradients. The computed layer emissivity is within 1% of that obtained by assuming a linear temperature relation.

Substituting Eq. (4) into Eq. (3) and integrating over the optical depth, we obtain two analytical expressions governing the upward and downward intensities

$$\begin{cases} \pi I^{+}(\tau,\mu) = m\tau + (B_b - \mu m)(1 - e^{-\tau/\mu}) \\ \pi I^{-}(\tau,\mu) = m[\tau - \tau_0 e^{(\tau_0-\tau)/\mu}] + (\mu m - B_b)[1 - e^{(\tau_0-\tau)/\mu}] \end{cases} \tag{5}$$

With further integration over the azimuthal angle and the respective zenith angle, we obtain the analytical solutions for emission from the layer top and layer bottom, and for total transmission and reflection

$$\begin{cases} E = B_t(1-T) - 2m(1-t-\tau_0 T)/3 \\ E^{*} = B_b(1-T) + 2m(1-t-\tau_0 T)/3 \\ T = 2E_3(\tau_0) \\ R = 0 \end{cases} \tag{6}$$

where $t = e^{-\tau_0}$ and E_3 is the exponential integral function of 3rd order.

Cloudy Layer

van de Hulst's similarity relations, which reduce the problem of anisotropic scattering to one of isotropic scattering by scaling the optical thickness and single scattering albedo, are adopted to treat the anisotropic scattering properties of aerosols and clouds. The scaling facter used is (1-g), i.e., the mean free path of a photon is less by a factor (1-g) than the value determined under the assumption of isotropic scattering (Hansen, 1969).

The two-stream approximation is then adopted to solve radiative transfer in an isotropic scattering medium. By dividing the radiation field into two streams according to Gaussian quadrature, Eq. (1) can be transformed to two coupled linear differential equations governing the upward and downward intensities I^+ and I^- (Wang and Domoto, 1974). Using the sum and difference of I^+ and I^-, denoted by X and Y respectively as dependent variables, we can derive two uncoupled second order linear differential equations

$$\begin{cases} \dfrac{d^2X}{d\tau^2} - 3a^2X(\tau) = -6a^2I_b(\tau) \\ \\ \dfrac{d^2Y}{d\tau^2} - 3a^2Y(\tau) = 2\sqrt{3}\, a^2 \dfrac{dI_b}{d\tau} \end{cases} \tag{7}$$

where $a^2 = 1 - \tilde{\omega}$.

Replacing I_b with Eq. (4), X and Y can be solved by the standard method of variation of parameters. The two-stream solutions for emission from the layer top and layer bottom, and for total transmission and reflection are then

$$\begin{cases} E = a(PB_t - mQ - B_b)/D \\ E^* = a(PB_b + mQ - B_t)/D \\ T = a/D \\ R = uv(e^{\tau_1} - e^{-\tau_1})/D \end{cases} \tag{8}$$

where

$$\begin{cases} P = ve^{\tau_1} + ue^{-\tau_1} \\ Q = ve^{\tau_1} - ue^{-\tau_1} - a \\ D = v^2 e^{\tau_1} - u^2 e^{-\tau_1} \\ u = (1-a)/2 \\ v = (1+a)/2 \\ \tau_1 = \sqrt{3}\, a\tau_0. \end{cases} \tag{9}$$

The optical thickness τ_0 and the single scattering albedo $\tilde{\omega}$ are given by

$$\begin{cases} \tau_0 = k u + \tau_s(1-g) + \tau_a \\ \tilde{\omega} = \tau_s(1-g)/\tau_0 \end{cases} \tag{10}$$

where k is the correlated gas absorption coefficient and u is the gas amount.

Figure 1 shows the percent error of computed layer emissivity in the window region based on the two-stream approximation and the exact multiple scattering calculations for isotropic scattering. In order to improve the accuracy of the two-stream approximation for isotropic scattering, we have obtained an empirical relation

$$F(\tilde{\omega}, \tau_0) = 1 + 0.14\, t + 0.10\tilde{\omega}^2 (1-t) + (-1.03 + 0.40\tilde{\omega} + 0.63\tilde{\omega}^2)\tau_0 t + (2.02 - 0.68\tilde{\omega} - 1.34\tilde{\omega}^2)\tau_0^2 t^2 + 0.45\, \tau_0^2 (\tau_0 - 1) t^{3/2} (1-\tilde{\omega}) \quad (11)$$

to multiply E and $E^{\bullet}$. This yields emissions which are within 2% of exact multiple scattering results for all values of $\tilde{\omega}$ and τ_0. Although this empirical relation is derived from window region results, it is applicable to other thermal regions as well.

First we examine the accuracy of applying the scaling isotropic scattering approximation to anisotropic scattering medium in the thermal region. Calculations are made for water cloud ($\tau_0 = 8$), ice cloud ($\tau_0 = 2$) and sulfuric acid aerosol particles ($\tau_0 = 0.1$). The cloud particle properties are defined in Section 3. A power law size distribution is assumed for aerosol particles with radius ranging from 0.1 to 10 μm (the mean radius is about 0.3 μm). The index of refractions is taken from Pollack et al. (1973). Based on Mie theory, the spectral scattering properties for cloud and aerosol particles are computed. Table 1 gives the calculated spherical albedo, transmission and absorption at 10 and 20 μm based on doubling and adding method, and the scaling isotropic scattering approximation. It can be seen that all the spherical quantities have the accuracy up to the third decimal point. Other spectral regions have similar results. Practically speaking the results of the scaling isotropic scattering approximation and the anisotropic scattering are nearly identical in the thermal infrared regions.

From above analyses we have obtained the analytic expression of emission, transmission and reflection function for clear and cloudy layers. When applying the adding method, these functions can be used for computing the fluxes at the interface of the layers (Lacis and Hansen, 1974). But, for terrestrial radiation,

there is an additional emission term which has to be included in the upward and downward addings. Therefore, in the following, we describe briefly the steps used to compute the monochromatic fluxes at given spectral interval $\Delta\nu_j$ for each value of correlated absorption coefficient k_n (cf. Fig. 2).

1) Using Eqs. (6), (8) and (9) the reflection R_ℓ, transimssion T_ℓ, optical thickness $\tau_{0\ell}$, upward emission E_ℓ and downward emission E^*_ℓ, $\ell = 1, L+1$ are computed for each layer.

2) Starting with the ground layer, the layers are added upward one at a time to obtain the composite upward flux U_ℓ,

$$U_\ell = E_\ell + \sum_{i=L'}^{\ell-1} E_i \; T \left(\sum_{k=i+1}^{\ell} \tau_k \right) \quad \text{for clear layer}$$

and

$$U_\ell = E_\ell + (U_{\ell-1} + E^*_\ell \bar{R}_{\ell-1}) T_\ell / (1 - R_\ell \bar{R}_{\ell-1}) \quad \text{for scattering layer,}$$

$L' = 1$ if atmosphere is clear and $L' = \ell$ if ℓ is the last scattering layer encountered in the process of upward adding. It is noted that $U_{L'}$ instead of $E_{L'}$ should be used in the upward addings after the scattering layer $\ell = L'$ is passed.

The reflection function $\bar{R}_\ell$ of composite layer 1 through ℓ is

$$\bar{R}_\ell = R_\ell + T_\ell \; \bar{R}_{\ell-1} \; T_\ell / (1 - R_\ell \; \bar{R}_{\ell-1})$$

3) Layers are added downward one at a time to obtain the composite downward flux D_ℓ,

$$D_\ell = E^*_{\ell+1} + \sum_{i=\ell+2}^{L'} E^*_i T \left(\sum_{k=\ell+1}^{i-1} \tau_k \right) \text{ for clear layer,}$$

and

$$D_\ell = E^*_{\ell+1} + (D_{\ell+1} + E_{\ell+1}\bar{R}^*_{\ell+1})T_{\ell+1}/(1-R_{\ell+1}\bar{R}^*_{\ell+1}) \text{ for scattering layer.}$$

The reflection function $\bar{R}^*_\ell$ of composite layer L+1 through ℓ+1 is

$$\bar{R}^*_\ell = R_{\ell+1} + T_{\ell+1}\bar{R}^*_{\ell+1}T_{\ell+1}/(1-R_{\ell+1}\bar{R}^*_{\ell+1})$$

L' = L+1 if atmosphere is clear and L' = ℓ+1 is the last scattering layer encountered in the process of downward adding. Same as step 2), $D_{L'}$ instead $E^*_{L'}$ should be used in the downward addings after the scattering layer $\ell = L'$ is passed. After each layer is added, step 4) is performed.

4) The upward and downward fluxes of the interface between two composite layers (1, ℓ) and (ℓ+1, L+1) are

$$\begin{cases} q_\ell = (U_\ell + D_\ell\bar{R}_\ell)/(1-\bar{R}_\ell\bar{R}^*_\ell) \\ q^*_\ell = (D_\ell + U_\ell\bar{R}^*_\ell)/(1-\bar{R}_\ell\bar{R}^*_\ell) \end{cases} \tag{12}$$

The total fluxes are found by summing over values of k-distribution function n and spectral interval j.

It is worthwhile to point out that in the present formulation, the product

of the transmissions in a clear atmosphere must be treated as the transmission for the sum of the optical paths traversed by the radiation, i.e.,

$$\pi_i T(\tau_i) = T(\sum_i \tau_i) = 2E_3(\sum_i \tau_i) \qquad (13)$$

because the solutions in Eq. (6) are in angle-averaged form. However, if Eq. (5) is used for combing layers, the product of the transmissions for the separate optical paths can be used.

b. Frequency integration

Frequency integration is used to compute total flux by summing over the monochromatic fluxes. For the earth's atmosphere, the frequency integration is very tedious and requires hundred and thousand monochromatic calculations because of the complicated molecular structures of the trace gases. Our approach to this problem is a generalization of the k-distribution method used by Lacis and Hansen (1974).

The k-distribution, f(k), for a given gas and frequency interval is the probability density function such that f(k)dk is the fraction of the frequency interval for which the absorption coefficient is between k and k+dk. The basic idea of grouping frequency intervals of gaseous spectra according to absoprtion coefficient strengths goes back at least to Ambartsumian (1936) who used it in estimating the influence of absorption lines in stellar atmosphere. This method allows the integration over wavelength for absorbing gases to be resolved implicitly by integrating the monochromatic solutions over k-distribution function. Lacis and Hansen (1974) used the k-distribution method to include the effects of multiple scattering. However, strictly speaking, this method is not applicable in an inhomogeneous atmosphere and the most commonly used

approximation is to scale the gas absorber amount according to local pressure and temperature (for example, see Lacis and Hansen, 1974). Wang et al. (1976) and Hansen et al. (1978) used a different approximation, which they called the correlated k-distribution method, by assuming that a simple correlation in frequency space of absorption coefficient at different temperatures and presures could be found. The approximate treatment is remarkably accurate as demonstrated by comparing with line-by-line calculations for the 9.6 μm ozone band (Lacis et al., 1979). It is found that the correlated k-distribution method gives the ozone heating rate within 0.1 K day^{-1} of line-by-line calculations while the commonly used pressure-scaling and Curtis-Godson approximations fail to yield accurate results (Walshaw and Rogers, 1963). Furthermore, the present method is several orders of magnitude faster than line-by-line calculations.

3. Atmospheric model

a. Spectral data

The solar and thermal spectrum are divided into 36 and 27 frequency intervals, respectively. Ten probability values are used for each interval. We have adopted the solar flux of Labs and Neckel (1968) as the insolation at the top of the atmosphere with a solar constant 1.958 cal $min^{-1}cm^{-2}$. The band model parameters of the major and minor atmospheric trace gases in the frequency intervals are computed based on fitting the calculated transmissions (line-by-line calculations with Voigt line profile if line data are available) with the Malkmus model at 3 temperature and 12 pressure levels applicable to the earth's atmosphere. Interpolations are made for pressures and temperatures other than the reference levels. Table 2 gives the major absorption bands of the trace gases used in the radiation model. In solar radiation regime, the principle gaseous absorbers in the earth's atmosphere are water vapor in the troposphere and ozone in the stratosphere. Water vapor absorbs primarily in the near-infrared region. At shorter wavelengths the main gaseous absorber is ozone which is effective in the ultraviolet and in the visible. Carbon dioxide, oxygen, nitrogen and nitrogen dioxide are minor contributors to the total atmospheric absorption. Fig. 3 taken from Pettit (1951) is representative of the spectral absorption for clear sky conditions. In the terrestrial radiation regime, water vapor, carbon dioxide and ozone are the major greenhouse ingredients. However other minor trace gases such as N_2O, CH_4, NH_3, etc., can have a significant effect on the atmosphere's thermal structure because they have strong absorption bands within the 7 - to 14-μm atmospheric window which transmits most of the thermal radiation from the earth's surface and lower atmosphere (Fig. 4).

The number of frequency intervals is sufficient to permit the spectral dependence of the cloud and aerosol particle properties which are relatively slowly varying functions. The cloud particle size distribution, which can be represented in terms of two physical parameters, the mean effective radius, r, and the effective variance, b, was taken from Hansen (1971). Values of these two parameters used in the present study are r = 10μm, b = 0.15 for water cloud and r = 25μm, b = 0.1 for ice cloud. The spectral properties for water droplets and ice spheres were computed from Mie theory at solar and thermal spectrum for which Irvine and Pollack (1968) tabulated optical constant of ice crystals and Hale and Querry (1973) gave spectral data for water. The normial aerosol model proposed by Toon and Pollack (1976) is adopted. The model which is designated for global average radiative transfer calculations assumes sea salt, soil (basalt) and sulfate particles in the troposphere with τ_0 = 0.120 and sulfate (75%H_2SO_4, 25%H_2O in solution) in the stratosphere with τ_0 = 0.005.

b. Characteristics of the atmosphere

We have adopted a globally-averaged model as standard model atmosphere for climate and sensitivity studies.[1] Characteristics of the model and the computed surface temperature, convection and water vapor column amount are shown in Table 3.

Three types of clouds -- high, middle and low -- are included and assumed to be non-overlapping. High cloud is assumed to be ice cloud while middle and low clouds are treated as water clouds. The cloud heights and cloud amounts are derived from the data compiled by London (1956), Sasamori et al. (1972) and Hoyt (1976), and are modified to allow for the non-overlapping assumption. However, no data is available for cloud optical thicknesses (at 0.55 μm) except for cirrus clouds in which τ_0 = 2 gives a corresponding visual albedo of

[1] A tropical model atmosphere can also be formulated simply by setting ocean and atmospheric meridional energy transport equal to observed values, and a thermal inertia appropriate for the upper ("mixed") layer of the ocean as illustrated in Hansen et al. (1978).

~20%. Therefore we choose τ_0 = 6 and 16, respectively, for middle and low water clouds strictly based on radiative-convective equilibrium calculations such that both values of the computed global albedo and surface temperature are close to observed values. The vertical extent of the cloud layer is assumed to be 1 km. The ocean mixed layer depth is assumed to be 73 m based on graphs published by Bathen (1972). The atmosphere is divided into 17 variable thickness layers from the surface to an altitude of 50 km. We use three Gauss divisions to perform integrations over angle for solar radiation while the solutions for terrestrial radiation are already in angle-averaged form. Solar and thermal radiative fluxes at each level are then computed by averaging over clear and cloudy regions.

Since no hydrology is included in the one-dimensional radiative-convective model, we perform the sensitivity study under the assumption of fixed relative humidity (FRH) and fixed absolute humidity (FAH). For the FRH assumption, if the temperature increases during climate change, the absolute humidity also increases, causing a substantial positive feedback effect ~1.5 (cf. Wang et al., 1976). In the present study, we adopted the formulation of relative humidity used by Manabe and Wetherald (1967). The relative humidity profile for $P/P_0 > 0.2$ is taken from Manabe and Wetherald [their Eq. (2)] while for $P/P_0 < 0.02$, it is computed based on constant 3 ppm mixing ratio and the temperature profile of midlatitude model atmosphere of McClatchey et al. (1972). Unless otherwise stated, we assume fixed relative humidity and fixed cloud altitude (see Section 5c) in our computations.

The vertical O_3 distribution is described by an analytic expression with coefficients specifying the maximum concentration height, the scale height and the total ozone amount (see footnote 32 of Wang et al. 1976). The total ozone column amount is taken from 10 years averaged data compiled by London et al. (1976), while the maximum concentration height and the scale height

are chosen from the seasonal and latitudinal ozone vertical distributions published by Dutsch (1974). We use ozone data at 40 N on April 15 as the standard ozone distribution in the unperturbed model atmosphere. The distribution is very similar to the one proposed by Krueger and Minznev (1976) for the 1976 U.S. Standard Atmosphere.

4. Radiative-convective equilibrium

Studies of radiative equilibrium of non-gray atmosphere have been carried out by Yamamoto (1953, 1955), Manabe and Moller (1961) and others. Because it neglects atmospheric motions, the model atmosphere always has a cooler upper troposphere and a higher surface temperature than observed. The observed temperature gradient or lapse rate in the earth's troposphere is primarily maintained by the convective processes and large scale eddies. Moist convection is dominant in determining the lapse rate in the tropics while large scale eddies which can be estimated by using baroclinic theory (Stone, 1972), are most important in mid-latitudes.

In the one-dimensional radiative-convective model the vertical transfer of heat is parameterized in such a way that the lapse rate computed based on radiative equilibrium can not exceed a critical lapse rate(Γ). In this parameterization, convection is invoked to set the lapse rate in the convecting region equal to Γ. This simple convective adjustment process approximates the actual heat transport by atmospheric motions, thereby permitting a more realistic temperature distribution throughout the atmosphere (Manabe and Strickler, 1964).

In the numerical computations, the radiative-convective equilibrium is approached by a time-marching procedure as follows:[2]

(1) The radiative temperature change of atmospheric layers is calculated from solar radiative heating and thermal radiative cooling which were computed from the flux divergence. Surface temperature is computed based on energy balance among thermal, solar and convective fluxes. The convective flux is calculated from stability criteria using previous time step surface temperature and the new radiative equilibrium atmospheric temperature. (2) Before using the new temperatures for radiative flux calculations, the lapse rate is checked against Γ, beginning

[2]This time-marching procedure adopted in the present model allows us to study time-dependent radiative perturbation. For example, Hansen et al. (1978) studied the temperature changes caused by the large increases in stratospheric aerosols after the explosive eruption of Mount Agung in 1963.

from the surface with the new surface temperature. If the new temperature distribution is not stable in any given layer, then a convective flux is required in order to maintain a stable atmosphere.

(3) The new temperature distribution, along with the computed water vapor amount if FRH is assumed, are used to calculate radiative fluxes and heating rates.

(4) Processes (1) - (3) are repeated until a steady state is reached. At steady state, the layer without convection will be in radiative equilibrium with zero net flux, while others will be in radiative-convective equilibrium with convection supplied from the surface.[3] The surface is in energy balance with the excess of net downward solar radiation over net upward long-wave radiation equal to the convective heat flux required to maintain a stable atmosphere.

Fig. 5 shows the computed radiative-convective equilibrium temperature distribution for two Γ values -- a constant 6.5 K km^{-1} and a moist-adiabatic lapse rate (see next sectionfor detailed discussions of the sensitivity of model result to Γ). In the middle and upper stratosphere, the temperature structure is very similar for the two Γ values. But in lower stratosphere and troposphere, the two temperature distributions are quite different and they cross over around 6 km. However, thecomputed equilibrium surface temperatures for the two models are very close with 287.39 K for 6.5 K km^{-1} and 287.80 K for an assumed moist-adiabatic lapse rate. The U.S. standard atmosphere temperature

---

[3]Typically, total convection is supplied fromthe surface because a two-zone atmosphere exists, i.e., a radiative-convective equilibrium (RCE) troposphere and a radiative equilibrium (RE) stratosphere. However if the troposphere has two or more zones, for example, a RCE-RE-RCE troposphere caused by a cloud or dense aerosol layer, the convection needed above the RE region can be partially supplied by this region with additional energy provided by the surface. The treatment actually simulates a small scale energy transport. In the numerical scheme, this readjustment of convection in order to eliminate the more than two-zone atmosphere takes place in step (2) of the time-marching procedures.

profile is also shown. A difference of 8 K is found around the tropopause region where, according to observations, dynamics plays a major role. In the middle and upper stratosphere, where ozone absorption of solar radiation is the main heat source, model temperatures are generally cooler by 5K than the U.S. standard atmosphere. This is partly due to cooler tropopause temperature and also partly caused by the uncertainty in the ozone distribution between 1-10 mb.

5. Sensitivity study of radiative-convective model

In this section, the sensitivity of the model results to the parameters used in the radiative-convective model is studied. The purpose is to examine how the model atmosphere responds to different values of assumed model parameters such as critical lapse rate, clouds and humidity. Because of the importance of carbon dioxide in atmospheric radiative transfer and its role played in global climate (Schneider, 1975; Manabe and Wetherald, 1975), we also examine the model sensitivity to these parameters withthe carbon dioxide concentration increased by a factor of two.

a. Critical lapse rate

The computed thermal structure of the earth's atmosphere depends strongly on the assumed values of Γ which is generally taken to be a constant value of 6.5 K km^{-1} in the radiative-convective model. Recently, Rennick (1977) has analyzed the zonal averaged temperature of the earth's atmosphere and finds that the temperature structure is dependent upon latitude during any given season, and its seasonal variation is different at different latitudes. However, as pointed out by Ramanathan and Coakley (1978) and Stone and Carlson (1978), the hemispheric mean lapse rates are in good agreement with the moist-adiabatic lapse rate in the lower troposphere while they are closer to constant 6.5 K km^{-1} in the upper troposphere.

Fig. 6 shows the computed surface temperature as a function of critical lapse rate. In general, larger lapse rate value yields higher surface temperature since the needed vertical transport of heat by convective processes is smaller. The atmosphere reaches radiative equilibrium if the critical lapse rate value increases indefinitely. On the other hand, it is probably

not realistic to have critical lapse rate values less than moist-adiabatic lapse rate unless the large scale motions dominate the heat transport. We have also shown the surface temperature with the present-day carbon dioxide concentration increased by a factor of two. For $\Gamma = 6.5$ K km^{-1} the increases of carbon dioxide produces a 2.0 K surface warming which is very close to the results of 1.95 K by Manabe (see Schneider 1975) and 1.98 K by Augustsson and Ramanathan (1977); the surface temperature increases by 1.25 K if constant absolute humidity is used. The surface temperature change is slightly larger for larger Γ values because of the water vapor greenhouse effect as well as the overlapping of water vapor with carbon dioxide.

As discussed earlier, it is interesting to find that the moist-adiabatic atmosphere has a surface temperature close to the fixed 6.5 K km^{-1} lapse rate atmosphere, even though the thermal structure for the two atmospheric models are different (the computed total convection, total column water vapor amount and mean lapse rate for the moist-adiabatic atmosphere are 0.165 ly min^{-1} 1.95 cm and 5.48 K km^{-1} respectively). This is primarily caused by the cross-over of the two lapse rate profiles in the middle of the troposphere which affects the thermal structure but incidently maintains very similar surface temperature. It further demonstrates that for the study of climate even in a one-dimensional model, a fully interactive atmosphere model should be used rather than one based solely on the aspect of energy balanced at the top of the atmosphere. For a moist-adiabatic atmosphere, the Γ distribution in the atmosphere is mainly responsible for the smaller ΔT_s value which is 1.37 K for FRH and 0.77 K for FAH as shown in Fig. 6. In addition to the ice-albedo amplifications effect, this lapse rate effect may partially be responsible for the large CO_2 climate effect found in high latitudes in general circulation models (Manabe and Wetherald, 1975). The results we presented give a good indi-

cation of the uncertainty of the climatic effects due to increases of carbon dioxide to Γ inherent in the one-dimensional radiative-convective model. It also illustrates the complex nature of the climate system we are dealing with.

b. Humidity

Similar to previously discussed critical lapse rate the actual equilibrium response of the water vapor profile is one of the aspects that must be addressed in a more realistic modeling effort. However, the assumption of constant relative humidity should be a realistic approximation (Manabe and Wetherald, 1967, 1975). FRH has a much larger effect than FAH because of the increases of water vapor greenhouse effect. The substantial difference is clearly an indication of the uncertainty introduced by this assumption. In Fig. 7 we illustrate the sensitivity of surface temperature to surface relative humidity q_s. As expected, the higher the q_s, the warmer the surface. The change of surface temperature to change of q_s, dT_s/dq_s, is found to be 10.3 K. This sensitivity increases slightly to 11.1 K if the carbon dioxide concentration is doubled.

C. Cloud

Clouds play an important role in the radiation balance of the atmosphere. The presence of clouds considerably reduces the net radiation, while the atmospheric emission increases. The net radiative effect on the surface temperature is a cancellation between cooling caused by a higher albedo in the solar region and a warming due to an enhancement of greenhouse effect in the thermal region. Observations (Cox 1971; Fleming and Cox 1974) indicate that low and middle level clouds generally cool the surface and high cirrus clouds either warm or cool the surface depending on the cloud height as well as their optical properties. However, recently Lacis et al. (1979) made a detailed study of cirrus clouds using more realistic cirrus cloud properties. They found cirrus clouds are predominant greenhouse materials and cause warming at middle and upper troposphere in both low and high latitudes.

The requirements on the knowledge of cloud heights, amount, type, etc., for radiation calculations are formidable. However, for the purpose of simulating a relatively realistic atmosphere for a cloud sensitivity study, we adopt a simple cloud model which includes a single cloud layer as well as a more sophisticated model which has three cloud layers representing high, middle and low level cloud. It is our intention to study the sensitivity of surface temperature to changes in cloud amount, cloud top and base height, and the number of cloud layers in a radiative-convective model.

First we examine the effect of cloud amounts. The sensitivity of surface temperature to changes in high, middle and low cloud amounts, i.e., dT_s/dC is found to be 32.3, -12.3 and -51.6 K respectively. The results are based on the standard model atmosphere specified in Table 3 with a fixed relative humidity. In the earth's atmosphere, we do not anticipate a variation in cloud amount without having feedback from other dynamical processes. Consequently, these results merely illustrate the model sensitivity to the cloud amount used. The increases in high cloud amount heat up the sur-

face since the greenhouse effect is larger than albedo effect. On the other hand, low and middle level clouds cool off the surface if the cloud amounts increase. It is interesting to note that the warming due to doubling the carbon dioxide concentration will be in balance with the cooling induced by 0.06 reduction of cirrus cloud amount. Although the radiative effect of cirrus cloud is highly dependent upon the cloud model used as pointed out by Manabe and Wetherald (1967), the results indicate the importance of the role that cirrus clouds play in climate change. For example, Dickinson et al. (1978) have examined the effect of clorofluoromethanes on zonal atmospheric temperatures in the NCAR General Circulation Model. They found that the temperature of the tropical tropopause could increase by 2.5 K if the 1975 chlorofluoromethane emissions continued indefinitely. The higher temperature would likely allow water vapor concentrations in the stratosphere to build up. At the same time it is not clear whether the cirrus cloud amount would be increased or decreased. Judging from its large radiative effect one would admit that this potential problem can not be overlooked. The increases in low and middle level water cloud amounts by 0.05, as expected, decrease the surface temperature by 2.60 and 0.62 K respectively because the albedo effect dominates. The reduction of low cloud has a larger effect, since the cloud optical thickness is larger and the cloud is closer to the surface (Lacis et al., 1979). It is also found that similar linear relationships exist between the surface temperature change and the variation of cloud fraction if the carbon dioxide concentration is doubled.

Next, we study the sensitivity of model results to the number of cloud layers used. For this purpose, we have constructed a single-cloud model bearing no relation to the three-cloud model (see Cess 1974 for the discussions of correlation of three-cloud model to single-cloud model). This model assumes the cloud amount, cloud optical thickness, and cloud top altitude to be 50%, 10, and 6.0 km, respectively. Despite a higher global albedo of 0.328, the surface

temperature for the single-cloud model is 288.69 K. The higher surface temperature is caused mainly by the smaller amount of convection 0.149 ly min^{-1} needed because the absence of low cloud makes the troposphere more stable. As shown in Table 4 a doubling of the carbon dioxide concentration under the assumption of fixed cloud top and base altitude(FCA)is found to yield 1.75 K surface warming for the single-cloud model instead of 2.04 K obtained for the three-cloud model. This is due primarily to smaller water vapor amplification as can be seen from very similar results obtained for the FAH assumption. The warming effect is enlarged to 3.01 and 2.94 K respectively for the two models if the cloud top and base temperatures(FCT)are held fixed (Cess, 1974). The basic reasons for this substantial difference can be explained that for FCT the cloud altitudes increase for increasing surface temperature which in turn reduces the cooling effect on the surface by clouds (Lacis et al., 1979).

We have also examined the cloud base feedback effect. Two cases are studied, one for constant cloud top temperature and cloud base altitude (FCTT) and the other for constant cloud top altitude and cloud base temperature (FCBT). In both cases, they produce larger positive feedback than FCA. It is interesting to note that cloud top feedback is more important in single-cloud model while cloud base has larger feedback in three-cloud model. Compared to FCA assumption, the surface temperature change is enlarged by 72, 51 and 12%, respectively, for FCT, FCTT and FCBT assumptions in the single-cloud model. For the three-cloud model, this enhancement for the respective FCT, FCTT and FCBT assumptions is 44, 24 and 43%. These results are not surprising simply because clouds at different levels have different effects on surface temperatures as discussed earlier. The point we want to stress is that for climate studies, cloud base altitudes are equally important as cloud top altitudes.

For the purpose of understanding the cloud altitude-temperature feedback, it is worthwhile to examine the separate thermal, solar and dynamical effect arising fromthe changes in external parameter such as solar constant, and from the changes in internal parameter such as the increases of carbon dioxide concentra-

tion. The sensitivity of the model to such perturbation can be derived from the energy balance equations at the top and bottom of the present model atmosphere, i.e.,

$$F_s^+ = F_s^- + S_s + E_s \tag{14}$$

$$F_0 = \frac{S_0}{4}(1-\alpha) \tag{15}$$

where F_0 is the outgoing thermal flux at the top of the atmosphere, α is the global albedo. E_s is the total convective flux, and F_s^+, F_s^- and S_s are the upward thermal flux, downward thermal flux and downward net solar flux at the surface, respectively.

From Eq. (14), we can express the surface temperature change in terms of the individual thermal, solar and dynamical temperature change, i.e.,

$$\Delta T_s = (\Delta F_s^- + \Delta S_s + \Delta E_c)/ (F_s^+)' \tag{16}$$

where $(F_s^+)' = \frac{dF_s^+}{dT_s} = 4\sigma T_s^3$ if surface is assumed to be a black body in the thermal region and σ is the Stefan-Boltzmann constant. Table 4 presents the results for the two cloud models with carbon dioxide concentration doubled. It is found that the thermal contribution to total surface temperature change is overwhelming, with small negative feedback from solar and dynamical effects. For FAH, the dynamical temperature change is nearly cancelled out by solar temperature change. It is very clear that the increases of thermal downward flux caused by the increases of carbon dioxide concentration is the main reason for the higher surface temperature. The negative feedback from solar and convective fluxes are due to the increases of atmospheric solar absorption and the

decreases in atmospheric stability, respectively. One interesting feature which we mentioned earlier is that, compared to the three-cloud model, the single-cloud model has larger thermal effect for FCT and FCTT assumptions, and smaller thermal effect for FCA and FCBT assumptions. This feature can also be seen in the total surface temperature change.

From Eq. (15), a convenient measure of the global sensitivity to changes in solar constant can be defined as

$$\beta_0 = S_0 \frac{dT_s}{dS_0} = \frac{F_0}{\frac{dF_0}{dT_s} + \frac{S_0}{4}\frac{d\alpha}{dT_s}} \qquad (17)$$

where dF_0/dT_s and $d\alpha/dT_s$ are the respective thermal radiation and global albedo change to changes in surface temperature. Values of β_o for the present model for different cloud altitude feedbacks are given in Table 5. The results computed by Lian and Cess (1977) are also shown for comparison. It is found that FCT assumption in three-cloud model and FCTT assumption in single-cloud model give the value of dF_0/dT_s in close agreement with Lian and Cess' value, whose calculations included the most realistic latitudinal distribution of cloudiness, surface temperature and solar zenith angle. This result is consistent with the conclusion obtained by Cess (1974, 1976). However, the α-T_s feedback is zero in energy balance model while it has positive small value for FCT assumption and negative values for other cloud altitude-temperature feedback assumptions. In general, fixed cloud base temperature assumption yields larger β_0 values than the one computed based on

fixed cloud base altitude assumption because of the positive feedback induced by the increases in cloud base altitudes for the former case, which further enhances the surface warming. Compared to FCA assumption, the global sensitivity β_0 is amplified by 60, 42 and 8% in the single-cloud model and 23, -5 and 16% in the three-cloud model, respectively, for FCT, FCTT and FCBT assumptions. These results are qualitatively in agreement with the results found for the doubling carbon dioxide experiments. Therefore, one must be cautious to use the different cloud altitude feedbacks for climate studies because the enhancement in model sensitivity depends on the cloud model used.

6. Climatic effect of ozone reduction in the atmosphere

Ozone is of major importance in maintaining the thermal structure in the stratosphere through its absorption of solar ultraviolet and visible radiation and its effective blocking of the upwelling thermal emission from the earth's surface in the 10μm window region. A factor of two variation in ozone concentration at 45 km can affect the local temperature by ~ 5 K. In a similar manner but to a lesser extent ozone also affects tropospheric and surface temperature. In general, the larger the column amount of ozone or the lower the height of maximum ozone concentration, the warmer is the temperature of troposphere and surface (Manabe and Wetherald, 1967; Ramanathan et al., 1976b). The tropospheric and surface warming are caused mainly by the increases of thermal downward flux.

In recent years, there has been increasing concern as to the possibility of a reduction in the amount of stratospheric ozone due to photochemical reactions involving trace gases, especially the oxides of nitrogen (NO_x) and chlorofluoromethanes (CFMs). The concentrations of the trace gases may be increased due to the use of high-flying aircrafts, the use of agricultural fertilizers and the use of CFMs in aerosol sprays and refrigerators (CIAP, 1975; NAS, 1976; NASA, 1977). The potential climate effects associated with the increases of CFMs are the warming due to CFMs greenhouse effect and the cooling caused by the depletion of stratospheric ozone (Ramanathan, 1975; Wang et al., 1976). However, because of the extreme complexity of this problem, uncertainties regarding the ozone reduction in the stratosphere are still very great. Nevertheless, the matter deserves further thorough study since stratospheric ozone reduction has substantial long-term effects and in this study we emphasize these effects. First we examine the role ozone played in determining the surface temperature.

Table 6 shows the computed radiative-convective equilibrium surface temperature for three different ozone distributions corresponding to 0, 40 and 80 N at April 15. The total ozone amount for equator is a minimum and that for 80 N a maximum, while the height of the maximum concentration decreases toward higher latitudes. It is found that reducing the total ozone amount and increasing the height of maximum ozone concentration cools the surface, which is in qualitative agreement with published results (Manabe and Wetherald, 1967). Relatively speaking, the height of maximum ozone concentration, i.e., the shape of the ozone distribution has a larger effect on the surface temperature than the total amount as can be seen from the computed surface temperatures for 0 and 80 N with the distributions normalized to the total ozone amount of 40 N. This further suggests that ozone reduction at different altitudes has different effects on surface temperature. For this purpose, we have performed a sensitivity study of ozone reduction in the atmosphere (Wang et al., 1979b). It is found that the region which has the largest effect on surface temperature due to ozone reduction is around the tropopause where ozone causes thermal heating instead of cooling (see Lacis et al., 1979). The reduction of ozone in this region has a factor of two to three larger effect on surface temperature compared to other parts of the atmosphere.

Table 7 gives the unperturbed model atmospheres and the changes in thermal structure due to stratospheric ozone reduction. As expected the addition of aerosols increases the global albedo and decreases the surface temperature if the globally-averaged aerosol model proposed by Toon and Pollack (1976) is used. The surface temperature is decreased by 1.43K, which is consistent with the 2.23 K surface cooling obtained by Wang and Domato (1974) with a tropospheric aerosol optical depth of 0.223. The temperature at 60 mb decreases by 33 K if total stratospheric ozone is removed between 12 and 50 km. However a 25% reduction in ozone concentrations decreases the 60 mb temperature by only 2.73 K. This small temp-

erature variation is caused by the strong ozone absorbing bands in the ultraviolet which is saturated for 0.5 cm of ozone (Lacis and Hansen, 1974). A total removal of stratospheric ozone cools the surface by 1.0 K irrespective of the presence or absence of aerosols. This demonstrates that reduction of stratopsheric ozone alone always cools the tropospheric and surface temperature with or without the presence of tropospheric aerosols.

Previous analyses emphasize on the study of stratospheric ozone column reduction. These is also the possibility that at particular altitudes the local change in ozone is much larger or smaller than the average for the total column. Large perturbations in the ozone profile might have their own effects through perturbation of temperature. For this purpose, we have studied ozone reduction in the atmosphere caused by increases of $CFCl_3$ and CF_2Cl_2 emissions.

Based on a standard one-dimensional photochemical model, Yung et al. (1979) have calculated the unperturbed and perturbed ozone concentration profiles. The unperturbed reference profile is based on 0.11 ppbv $CFCl_3$ and 0.21 ppbv CF_2Cl_2 which reflect present-day concentrations (NASA, 1977). According to NAS (1976) the projected concentration increases of chlorofluoromethanes at year 2030 can be a factor of ten or larger. In this study, we calculate the perturbed ozone profile based on 0.8 ppbv $CFCl_3$ and 2.3 ppbv CF_2Cl_2. The percentage ozone concentration change of the perturbed profile to the unperturbed, along with the computed equilibrium temperature change, are shown in Fig. 8. The total ozone column reduction is about 18%. A 7 K cooling is found in the 40 km region where the reduction of ozone concentrations is largest, ~50%. The tropospheric warming of 0.07 K is caused mainly by the increases of CFM concentrations (a 0.17 K cooling is found if CFMs maintain same concentration levels as used in unperturbed model). We have also used the moist-adiabatic lapse rate in this study. The stratospheric temperature change is similar to the one

shown in Fig. 8. However, the tropopause warming is enlarged to 0.13 K and surface temperature increased by 0.05 K instead of 0.07 K for a fixed 6.5 K km^{-1} lapse rate case.

7. Conclusions

In this paper, we present a one-dimensional radiative-convective model of the earth's atmosphere for climate studies. The sensitivity of the physical parameters inherited in the climate system such as lapse rate, humidity and clouds is examined. Because of its large climate effect, the increase of carbon dioxide concentration in the earth's atmosphere is used as a radiative perturbation for the sensitivity study of these model parameters. It is found that the surface warming of about 2K due to doubling carbon dioxide concentration depends weakly on cloud model (without cloud altitude-temperature feedback) and surface humidity values used. However, the critical lapse rate has a dominant effect on the surface temperature change. For example, the 2K surface warming is obtained based on constant 6.5 K km^{-1} lapse rate while dry-adiabatic lapse rate can result in a 2.5K increase in surface temperature. On the other hand, moist-adiabatic lapse rates which are close to observed values yield a much smaller warming of 1.4 K. We conclude that critical lapse rate values can make the climate effects due to increases of carbon dioxide concentration differ by a factor of two. It is also shown that the cloud base altitude feedback is equally important as the cloud top altitude feedback in climate studies. For example, compared to FCA assumption, the surface temperature perturbation due to increase of carbon dioxide concentration is amplified by 72, 51 and 12% respectively, for FCT, FCTT and FCBT assumptions in a single-cloud model. But the enhancement is found to be 44, 24 and 43%, respectively, in a three-cloud model. The enhancement in global sensitivity to changes in solar constant due to this feedback is qualitatively similar to the case of increasing carbon dioxide concentration. We conclude that the cloud-altitude feedback responds differently and depends on the cloud model used.

As a sample application of the present one-dimensional radiative-convective mdel, we have studied the climatic effects due to ozone reduction in the stratosphere. We have found that ozone depletions in stratosphere always cool both the stratosphere and the surface irrespective of the presence or absence of aerosol layers. However, the chlorofluoromethane-induced ozone column reduction at year 2030 following the current rate of chlorofluoromethane emissions, is about 18% and decreases the temperature by 7K around 40 km while the surface temperature increases by 0.07 K because of the greenhouse effects of chlorofluoromethanes.

Despite the lack of several major feedback mechanisms such as cloud cover feedback, surface albedo temperature feedback, the one-dimensional radiative-convective climate models provide adequate, at least first order, response of radiative perturbations in the earth's atmosphere. Recently Wang and Stone (1979a) have demonstrated that the ice-snow albedo-temperature feedback can be incorporated in the one-dimensional radiative-convective models in a realistic way. This addition greatly increases the model's ability for climate studies. As to other feedback mechanisms, they must wait for better understanding of the physical processes which control the different feedbacks.

ACKNOWLEDGEMENT

We thank James E. Hansen for useful discussions, and Y.L. Yung and J.P. Pinto for providing the vertical ozone distributions in the study of effect due to increases of chlorofluoromethanes.

REFERENCES

Ambartsumian, V., 1936: The effect of the absorption lines on the radiative equilibrium of the outer layers of the stars. Publications de L'Observatoire Astronomique de Leningrad, 6, 7-18.

Augustsson, T., and V. Ramanathan, 1977: A radiative-convective model study of the CO_2 - climate problem. J. Atmos. Sci., 34, 448-451.

Bathen, K.H., 1972: On the seasonal changes in the depth of the mixed layer in the North Pacific Ocean. J. Geophys. Res., 77, 7138-7150.

Burch, D.E., 1970: Semi-Annual Technical Report, Investigation of the absorption of infrared radiation by atmospheric gases. Aeronutronic Report U-4784 (Aeronutronic Div., Philco-Ford Corporation, Newport Beach, California.)

Cess, R.D., 1974: Radiative transfer due to atmospheric water vapor: Global considerations of the earth's energy balance. J. Quant. Spectr. Radiat. Transfer, 14, 861-871.

_____, 1976: Climate change: An appraisal of atmospheric feedback mechanisms employing zonal climatology. J. Atmos. Sci., 33, 1831-1843.

Chandrasekhar, S., 1960: Radiative transfer. New York, Dover, 393 pp.

CIAP Monograph 1, 1975: The natural stratosphere of 1974. Report DOT-TST-75-51. Dept. of Transportation, Washington, D.C.

Cook, C.F., W.B. Person, and L.C. Hall, 1967: Absolute infrared intensities of the fundamental absorption bands in solid CCl_4. Spectrochim. Acta Part A, 23, 1425-1433.

Cox, S.K., 1971: Cirrus clouds and the climate. J. Atmos. Sci., 28, 1513-1515.

Dickinson, R.E., T.M. Donahue and S.C. Liu, 1977: Effect of Chlorofluoromethane infrared radiation on zonal atmospheric temperatures. NCAR/0301/77-23.

Dickson, A.D., I.M. Mills, and B. Crawford, Jr., 1957: Vibrational intensities. VIII. CH_3 and CD_3 Chloride, Bromide, and Iodide. J. Chem. Phys., 27, 445-455.

Dütsch, H.U., 1974: The ozone distribution in the atmosphere. Can.J.Chem.Eng., 52, 1491-1504.

Fleming, J.R., and S.K. Cox, 1974: Radiative effects of cirrus clouds. J. Atmos. Sci., 31, 2182-2188.

Fowle, F.E., 1915: The transparency of acqueous vapor. Astrophys. J., 42, 394-411.

Goldman, A., F.S. Bonomo, W.J. Williams, and D.G. Murcray, 1975: Statistical-band-model analysis and integrated intensity for the 21.8μm bands of HNO_3 vapor. J. Opt. Soc. Am. 65, 10-12.

_____,T.G. Kyle, and F.S. Bonomo, 1970: Statistical band model parameters and integrated intensities for the 5.9μ, 7.5μ, and 11.3μ bands of HNO_3 vapor. AFCRL-70-0091.

Goody, R.M., 1964: Atmospheric Radiation: I. Theoretical Basis. Oxford University Press, 436 pp.

Hale, G.M., and M.R. Querry, 1973: Optical constants of water in the 220-nm to 200 μm wavelength region. Appl. Opts., 12, 555-563.

Hall, T.C., and F.E. Blacet, 1952: Separation of the absorption spectra of NO_2 and N_2O_4 in the range of 2400-5000 A. J. Chem. Phys., 20, 1745-1749.

Handbook of Geophysics, 1961: New York, The MacMillan Co.

Hansen, J.E., 1969: Absoprtion-line formation in a scattering planetary atmosphere: a test of van de Hulst's similarity relations. Astrophys. J., 158, 337-349.

_____, 1971: Multiple scattering of polarized light in planetary atmospheres. Part II. Sunlight reflected by terrestrial water clouds. J. Atmos. Sci. 28, 1400-1426.

_____, W.C. Wang, and A.A. Lacis, 1978: Mt. Agung eruption provides test of a global climate perturbation. Science, 199, 1065-1068.

Hoyt, D.V., 1976: The radiation and energy budgets of the earth using both ground-based and satellite-derived values of total cloud cover. NOAA TR ERL 362-ARL 4.

Irvine, W.M., and J.B. Pollack, 1968: Infrared optical properties of water and ice spheres. Icarus, 8, 324-360.

Krüeger, A.J., and R.A. Minzner, 1976: A mid-latitude ozone model for the 1976 U.S. Standard Atmosphere. J. Geophys. Res., 81, 4477-4481.

Labs, D., and H. Neckel, 1968: The radiation of the solar photosphere from 2000 Å to 100 μ. Astrophys. J., 69, 1-73.

Lacis, A.A., and J.E. Hansen, 1974: A paramterization for the absorption of solar radiation in the earth's atmosphere. J. Atmos. Sci., 31,118-133.

_____, W.C. Wang, and J.E. Hansen, 1979: Correlated k-distribution method for radiative transfer in climate models: application to effect of cirrus clouds on climate. Fourth NASA Weather and Climate Program Science Review, 309-314.

Lian, M.S., and R.D. Cess, 1977: Energy balance climate models: a reappraisal of of ice-albedo feedback. J. Atmos. Sci., 34, 1058-1062.

London, J., 1956: A study of the atmospheric heat balance. Final report, College of Engineering, New York Unviersity, 99 pp., Contract AF 19 (122) - 165.

_____, R.D. Bojkov, S. Oltmans, and J.I. Kelley, 1976: Atlas of the global distribution of total ozone, July 1957-June 1967. NCAR/TN/113+STR.

Ludwig, C.B., R. Bartle, and M. Grigg, 1969: NASA Contract Rep., CR-1380.

Manabe, S., and F. Moller, 1961: On the radiative equilibrium and heat balance of the atmosphere. Mon. Wea. Rev., 89, 503-532.

_____, and R.F. Strickler, 1964: Thermal equilibrium of the atmosphere with a convective adjustment. J. Atmos. Sci., 21,361-385.

_____, and R.T. Wetherald, 1967: Thermal equilibrium of the atmosphere with a given distribution of relative humidity. J. Atmos. Sci. , 24,241-259.

_____, and _____, 1975: The effects of doubling the Co_2 concentration on the climate of a general circulation model. J. Atmos. Sci., 32, 3-15.

McClatchey, R.A., R.W. Fenn, J.E.A. Selby, F.E. Volz, and J.S. Garing, 1972: Optical properties of the atmosphere. (Third edition). AFCRL-72-4097.

_____, W.S. Benedict, S.A. Clough, D.E. Burch, R.F. Calfee, K. Fox, L.S. Tothman, and J.S. Garing, 1973: Air Force Comb. Res. Lab. Rep., AFCRL-TR-73-0096.

NAS Report, 1976: Halocarbons: Effects on stratospheric ozone. National Academy of Sciences, Washington, D.C.

NASA, 1977: Chlorofluoromethanes and the stratosphere. R.D. Hudson, Ed., NASA, Washington, D.C.

Pettit, E., 1951: The Sun and Stellar Radiation in Astrophysics, T. Hynek, Ed. New York, McGraw-Hill, 703 pp.

Pollack, J.B., O.B. Toon, and B.N. Khare, 1973: Optical properties of some terrestrial rocks and glasses. Icarus, 19, 372-389.

Ramanathan, V., 1975: Greenhouse effect due to chlorofluorocarbons climatic implications. Science, 190, 50-52.

_____, 1976a: Radiative transfer within the earth's troposphere and stratosphere: A simplified radiative-convective model. J. Atmos. Sci., 33, 1330-1346.

_____, L.B. Callis, and R.E. Boughnev, 1976b: Sensitivity of surface temperature and atmopsheric temperature to perturbations in the stratospheric concentration of ozone and nitrogen dioxide. J. Atmos. Sci., 33, 1092-1112.

_____, and J.A. Coakley, Jr., 1978: Climate modeling through radiative-convective models. Rev. Geophys. Space Phys., 16, 465-489.

Rennick, M.A., 1977: The parameterization of tropospheric lapse rates in terms of surface temperature. J. Atmos. Sci., 34, 854-862.

Roberts, R.E., J.E.A. Selby, and L.M. Biberman, 1976: Infrared continuum absorption by atmospheric water vapor in the 8-12μm window. Appl. Opt. 2085-2090.

Saeki, S., M. Mizuno, and S. Kondo, 1976: Infrared absorption intensities of methane and fluoromethanes. Spectrochim. Acta, 32A, 403-413.

Sasamori, T., J. London, and D.V. Hoyt, 1972: Radiation budget of the southern hemisphere. Meteor. Monographs, 13, 9-23.

Schneider, S.H., and R.E. Dickenson, 1974: Climate modeling. Rev. Geophys. Space Phy., 12, 447-493.

_____, 1975: On the carbon dioxide-climate confusion. J. Atmos. Sci., 32, 2060-2066.

Stone, P.H., 1972: A simplified radiative-dynamical model for the static stability of rotating atmospheres. J. Atmos. Sci., 29, 405-418.

_____, and J.H. Carlson, 1979: Atmospheric lapse rate regimes and their parameterization. J. Atmos. Sci., 36, 415-423.

System, Science and Software, 1972: The effects of mezo-scale and small-scale interactions on global climate. AD-739 541.

Toon, O.B., and J.B. Pollack, 1976: A global average model of atmospheric aerosols for radiative transfer calculations. J. Appl. Meteor., 15, 225-246.

van de Hulst, H.C., 1963: A new look at multiple scattering. Goddard Institute for Space Studies, NASA, New York.

Varnanasi, P., 1976: Intensity measurements in freon bands of atmospheric interest. J. Quant. Spectrosc. Radiat. Transfer, 17, 385-388.

Walshaw, C.D., and C.D. Rodgers, 1963: The effect of the Curtis-Godson approximation on the accuracy of radiative heating rate calculations. Quart. J. Roy. Met. Soc., 89, 122-130.

Wang, W.C., and G.A. Domoto, 1974: The radiative effect of aerosols in the earth's atmosphere. J. Appl. Meteor., 13, 521-534.

_____, and Y.L. Yung, A.A. Lacis, T. Mo, and J.E. Hansen, 1976: Greenhouse effects due to man-made perturbations of trace gases. Science, 194, 685-690.

_____, and P.H. Stone, 1979a: Incorporation of surface albedo-temperature feedback in a one-dimensional radiative-convective climate model. Fourth NASA Weather and Climate Program Science Review, 361-365.

_____, J.P. Pinto, and Y.L. Yung, 1979b: Climatic effects due to halogenated compounds in the earth's atomsphere. Submitted to J. Atmos. Sci.

Yamamoto, G., 1953: Radiative equilibrium of the earth's atmosphere: II. The use of Rosseland's and Chandrasekhar's means in the line absorbing case. Sci. Rept. Tohoku Univ., Ser. 5. (Geophys.), 6, 127-136.

Yung, Y.L., J.P. Pinto, R.T. Watson, and S.P. Sander, 1979: Atmospheric bromine and ozone perturbations in the lower stratosphere. Submitted to J. Atmos. Sci.

Table 1

Comparisons between anisotropic scattering (AI) and scaled isotropic scattering (SI). The results are obtained based on doubling and adding method.

Scatterer	λ(μm)	Albedo		Transmission		Absorption	
		AI	SI	AI	SI	AI	SI
Water Cloud	10	0.0313	0.0322	0.0125	0.0145	0.9562	0.9533
(τ_0 = 8)	20	0.0298	0.0311	0.0006	0.0004	0.9697	0.9683
Ice Cloud	10	0.0096	0.0117	0.2342	0.2353	0.7562	0.7530
(τ_0 = 2)	20	0.1020	0.1049	0.2464	0.2486	0.6516	0.6465
Sulfate	10	0.0003	0.0004	0.9882	0.9880	0.0115	0.0116
(τ_0 = 0.1)	20	0.0	0.0	0.9964	0.9965	0.0036	0.0035

Table 2

Absorbing bands of trace atmospheric constituents. The values of assumed present concentration refer to ground level. The assumed vertical profiles are given in Table 3.

Species	Band Center λ (μm)	Band Center ω (cm^{-1})	Band Designation	References	Assumed Present Concentration (ppmv)
H_2O	0.7	14318	a	Fowle (1915)	variable
	0.8	12565	$\nu_2 + 3\nu_3$		
	0.91	11032	ρσT	McClatchey et al.	
	1.14	8805	Φ	(1972)	
	1.38	7251	Ψ		
	1.87	5330	Ω		
	2.70	3756	χ		
	3.2	3125	$2\nu_2$		
	6.25	1600	ν_2		
	10	1000	Continuum	Roberts et al.	
	20	500	Continuum	(1976)	
	10 - ∞	0 - 1000	Rotational	McClatchey et al. (1972)	
CO_2	1.2	8293	$\nu_1+2\nu_2+3\nu_3$	McClatchey et al.	330
	1.43	6976	ν_3	(1972)	
	1.6	6250	$\nu_1+4\nu_2+\nu_3$		
	2.0	5104	$2\nu_1+\nu_3$		
	2.7	3715	$\nu_1+\nu_3$		
	4.26	2349	ν_3		
	10	1000	ν_3		
	15	667	ν_3		
O_2	0.13 - 0.31	31949-76923		Handbook of Geophysics (1961)	2.095×10^5
	0.69	14535	B	McClatchey et al.	
	0.76	13123	A	(1972)	
O_3	0.2 - 0.37	27027-50000	Hartley and Huggins	Handbook of Geophysics (1961)	variable
	0.43-0.76	13158-23256	Chappuis		
	9.6	1042	ν_3	McClatchey et al. (1972)	
	14	714	ν_2		
N_2	4	2500	Continuum	Burch et al. (1970)	7.905×10^5
NO_2	0.24-0.50	20000-41667		Hall and Blacet (1952)	variable
N_2O	7.78	1285	ν_1	McClatchey et al.	0.28
	17.0	588	ν_2	(1972)	
	4.5	2223	ν_3		

Table 2

CONTINUED

Species	Band Center λ (μm)	Band Center ω (cm^{-1})	Band Designation	References	Assumed Present Concentration (ppmv)
CH_4	7.66	1306	ν_4	McClatchey et al. (1972)	1.6
NH_3	10.53	950	ν_2	McClatchey et al. (1972)	6×10^{-3}
HNO_3	5.9	1695	ν_2	Goldman et al. (1970, 1975)	variable
	7.5	1333	$\nu_3 + \nu_4$		
	11.3	850	$\nu_5 + 2\nu_9$		
	21.8	459	ν_9		
C_2H_4	10.5	949	ν_7	Ludwig et al. (1969)	2×10^{-4}
SO_2	8.69	1151	ν_1	Ludwig et al. (1969)	2×10^{-3}
	7.35	1361	ν_3		
CCl_2F_2	9.13	1095	ν_1	Varanasi (1977)	1×10^{-4}
	8.68	1152	ν_6		
	10.93	915	ν_8		
CCl_3F	9.22	1085	ν_1	Varanasi (1977)	1×10^{-4}
	11.82	846	ν_4		
CH_3Cl	13.66	732	ν_3	Dickson et al. (1957)	5×10^{-4}
	9.85	1015	ν_6		
	7.14	1400	$\nu_2 + \nu_5$		
CCl_4	12.99	770	ν_3	Cook et al. (1967)	1×10^{-4}
CF_4	7.80	1283	ν_3	Saeki et al. (1976)	6×10^{-5}

Table 3

Characteristics of the atmospheric model employed as a standard for comparison.

Characteristic	Value
Surface pressure P_s	1013.25 mb
Surface Temperature T_s	287.39 K
Solar "Constant" S_0	1.958 ly min^{-1}
Critical lapse rate Γ	6.5 K km^{-1}
Convection	0.159 ly min^{-1}
Clouds*	
Low	$\tau_0 = 16$, $z_c = 3$ km, C = 0.30
Middle	$\tau_0 = 6$, $z_c = 5$ km, C = 0.10
High	$\tau_0 = 2$, $z_c = 9$ km, C = 0.10
Ocean	
Mixed layer depth	73 m
H_2O vapor abundance	
Column amount	1.67 pr. cm
Distribution	
$p = P/P_0 \leq 0.02$	see text
$p = P/P_0 > 0.02$	$q^{\dagger} = 0.75\ (p-0.02)/(1-0.02)$
CO_2 abundance	330 ppmv
O_3 Column amount	0.345 cm (see Text)
Minor trace gases	see Table 2 of Wang et al. (1976)
Aerosols*	
troposphere	$\tau_0 = 0.120$
stratosphere	$\tau_0 = 0.005$

*τ_0 is the optical thickness at 0.55 μm, z_c is cloud top altitude and C the cloud fraction. †Value q is the relative humidity taken from Manabe and Wetherald (1967).

Table 4

Effects of cloud-altitude feedback on surface tmperature perturbation ΔT_s (K) if carbon dioxide concentration is increased by a factor of two. Separate thermal, dynamical and solar effect on surface temperature is calculated by computing the difference between unperturbed and perturbed cases. Total surface temperature change is the sum of the three effects as indicated in Eq. (16). FCA and FCT refer to fixed cloud altitudes and fixed cloud temperatures respectively. FCTT and FCBT denote fixed cloud top temperature and base altitude and fixed cloud top altitude and base temperature respectively.

MODEL	PARAMETER	FCA		FCT	FCTT	FCBT
		FRH	FAH	FRH	FRH	FRH
Single-cloud	ΔT_s	1.75	1.17	3.01	2.65	1.96
	$\frac{\Delta F_s^-}{(F_s^+)'}$	2.34	1.17	3.69	3.43	2.49
	$\frac{\Delta E_c}{(F_s^+)'}$	-0.33	0.07	-0.28	-0.42	-0.24
	$\frac{\Delta S_s}{(F_s^*)'}$	-0.26	-0.07	-0.40	-0.36	-0.29
Three-cloud	ΔT_s	2.04	1.25	2.94	2.53	2.92
	$\frac{\Delta F_s^-}{(F_s^+)'}$	2.58	1.25	3.33	3.10	3.33
	$\frac{\Delta E_c}{(F_s^+)'}$	-0.26	0.08	-0.03	-0.25	-0.06
	$\frac{\Delta S_s}{(F_s^+)'}$	-0.27	-0.08	-0.36	-0.32	-0.35

Table 5

Comparison of the global sensitivity parameter β_0 [defined in Eq. (17)] to changes in solar constant between the energy balance model and the present model for current climate conditions.

MODEL	$\frac{dF_0}{dT_s}$ $Wm^{-2}C^{-1}$	$\frac{S_0}{4}\frac{d\alpha}{dT_s}$ $Wm^{-2}C^{-1}$	β_0(C)
Lian and Cess (1977)	1.63	0	147
a. Three-cloud model			
FCA	2.39	-0.237	110
FCT	1.70	0.044	135
FCTT	2.32	-0.053	104
FCBT	1.97	-0.128	128
b. Single-cloud model			
FCA	2.40	-0.205	103
FCT	1.38	0.005	165
FCTT	1.62	-0.079	146
FCBT	2.16	-0.106	111

Table 6

Computed surface temperature for three different ozone distributions. The total ozone amount at the three latitudes represents the daily value of April 15 obtained by averaging over the 10 years data compiled by London et al. (1976).

Latitude	Maximum Concentration Height (km)	Total Amount (cm)	T_s(K)	Albedo	T_s^*(K)
0	27	0.248	286.18	0.311	286.44
40 N	22	0.345	287.39	0.307	———
80 N	18	0.443	289.09	0.303	288.53

*Surface temperature if total ozone amount is normalized to the amount of 40N.

Table 7

Changes in thermal structure due to stratospheric ozone reduction.

parameter	Aerosol-free Atmosphere		Aerosol Atmosphere		
	UA	100%*	UA	25%*	100%*
Global Albedo	0.2954	0.0183	0.3068	0.0034	0.0187
Temperature K					
60 mb	209.67	-32.64	209.49	-2.73	-32.74
surface	288.82	-1.05	287.39	-0.29	-1.00
Convection ly min^{-1}	0.1625	0.0040	0.1594	0.0009	0.0042
Water vapor column amount	1.85	-0.14	1.67	-0.03	-0.12

*Changes in model results with respect to unperturbed atmosphere (UA) due to indicated percent reduction of stratospheric ozone concentration between 12 and 50 km.

FIGURE CAPTIONS

Fig. 1: Percent error of layer emissivity computed based on two-stream approximation and exact multiple scattering calculations for isotropic scattering. The computation is performed with 280 and 300 K as the layer surface temperatures in the 10 μm window. To improve the accuracy of the two-stream approximation for isotropic scattering, a parameterization [defined in Eq. (11)] is obtained to multiply E and E* in Eq. (8) so that the emissions are within 2% of exact multiple scattering results for all values of $\tilde{\omega}$ and τ_0.

Fig. 2: Illustration of the terms used in the computations of flux. The atmosphere is divided into sufficient number of homogeneous layers. The layer properties R, T, τ_0, E, and E* represent reflection, transmission, optical thickness, emissions at top and bottom of the layer, respectively. The fluxes at theinterface of the layer are computed for all values of n based on the adding of two composite layers as indicated in the text.

Fig. 3: Spectral energy curve of solar radiation at sea level and extrapolated outside the atmosphere, as given by Pettit (1951). The darkened areas represent gaseous absorption in the atmosphere.

Fig. 4: Transmission of thermal radiation by atmospheric gases for present-day abundances. The scale is expanded for the weak absorbers illustrated in the lowest panel. The arrows indicate the locations of the chlorofluoromethane and chlorocarbon bands, which are too weak to be visible.

Fig. 5: Radiative-convective equilibrium temperature distributions for the earth's atmosphere with two critical lapse rate values. The U.S. standard atmosphere temperature profile is also shown for comparison.

Fig. 6: Computed surface temperature as a function of constant critical lapse rate. Solid line depicts present-day carbon dioxide concentration while dashed line is based on 660 ppmv carbon dioxide concentration. The single cross and dot are for moist-adiabatic assumption which has atmospheric mean value for 5.48 $K\ km^{-1}$.

Fig. 7: Computed surface temperature as function of surface relative humidity values.

Fig. 8: Temperature changes due to CFM-induced ozone perturbations, including the direct thermal effect of the increased chlorofluoromethane abundance. Note that the scales for $\Delta T > 0$ and $\Delta T < 0$ are different.

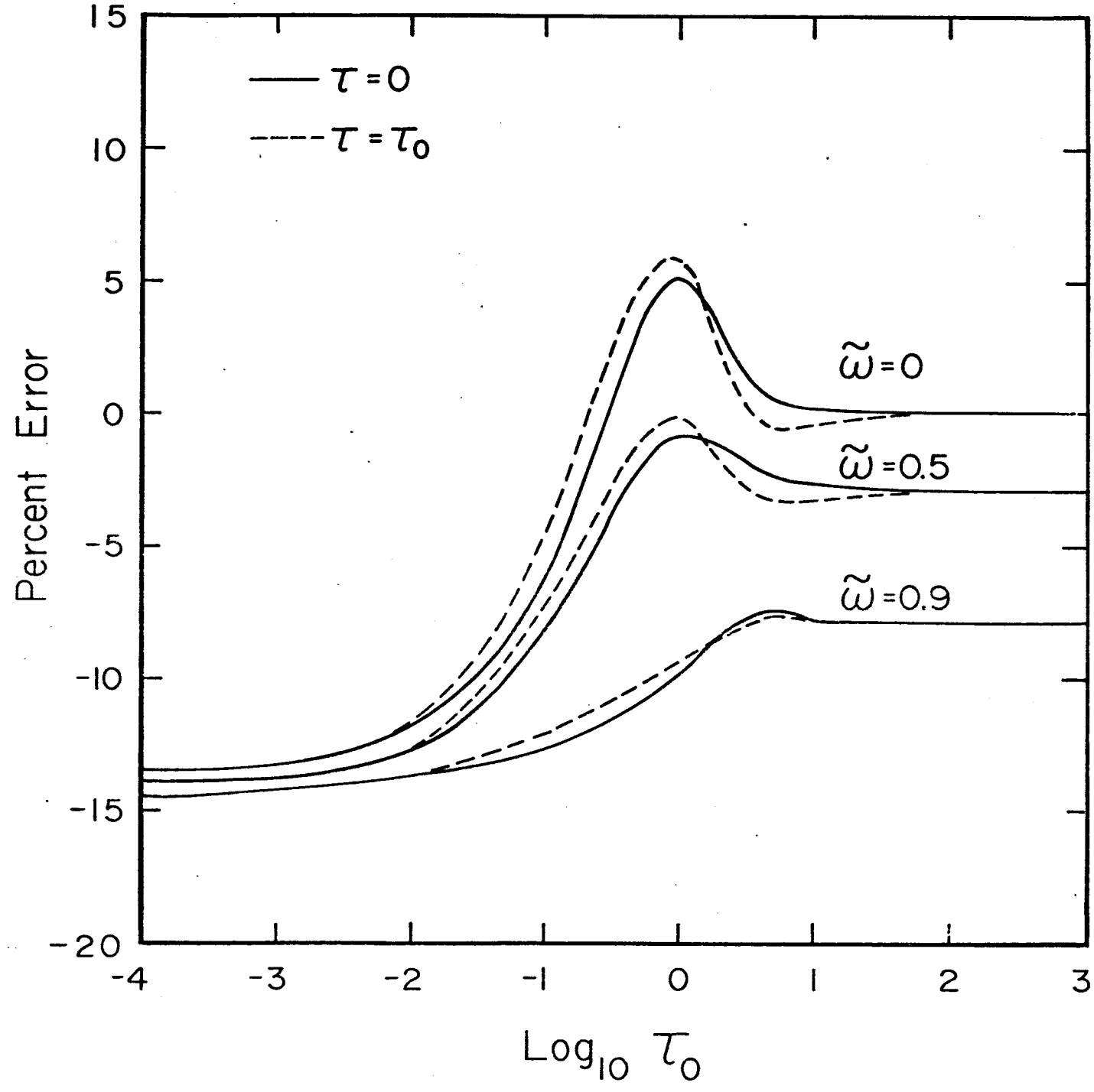
15
10
5
0
-5
-10
-15
-20
-4
-3
-2
-1
0
1
2
3
τ = 0
τ = τ0
ω̃ = 0
ω̃ = 0.5
ω̃ = 0.9
Percent Error
Log10 τ0

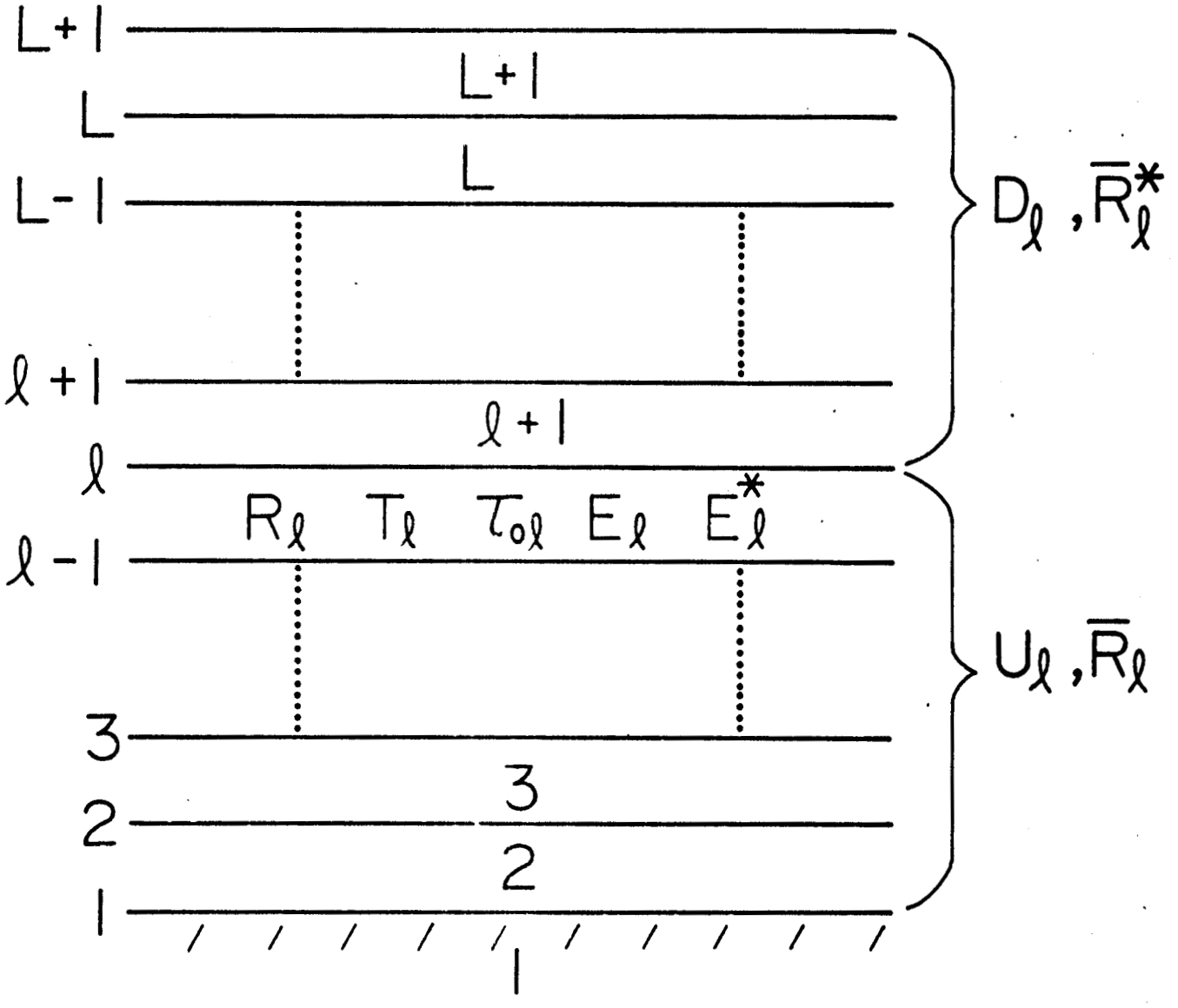
L+1
L+1
L
L
L-1
L
ℓ+1
ℓ+1
ℓ
R_ℓ T_ℓ $\tau_{o\ell}$ E_ℓ E_ℓ^*
ℓ-1
3
3
2
2
1
1
D_ℓ , $\bar{R}_\ell^*$
U_ℓ , $\bar{R}_\ell$

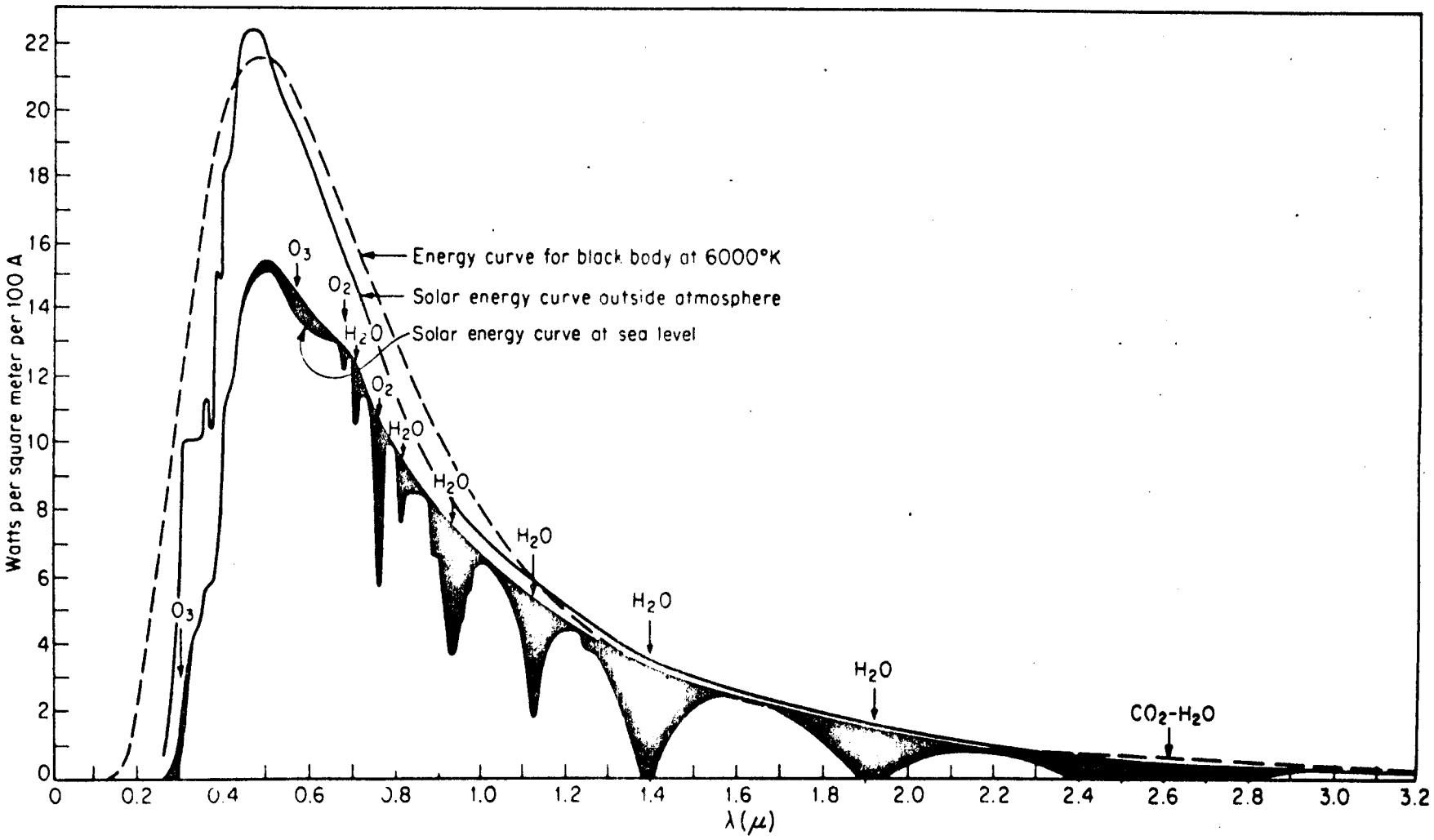
Watts per square meter per 100 A
λ(μ)
Energy curve for black body at 6000°K
Solar energy curve outside atmosphere
Solar energy curve at sea level
O3
O2
H2O
CO2-H2O

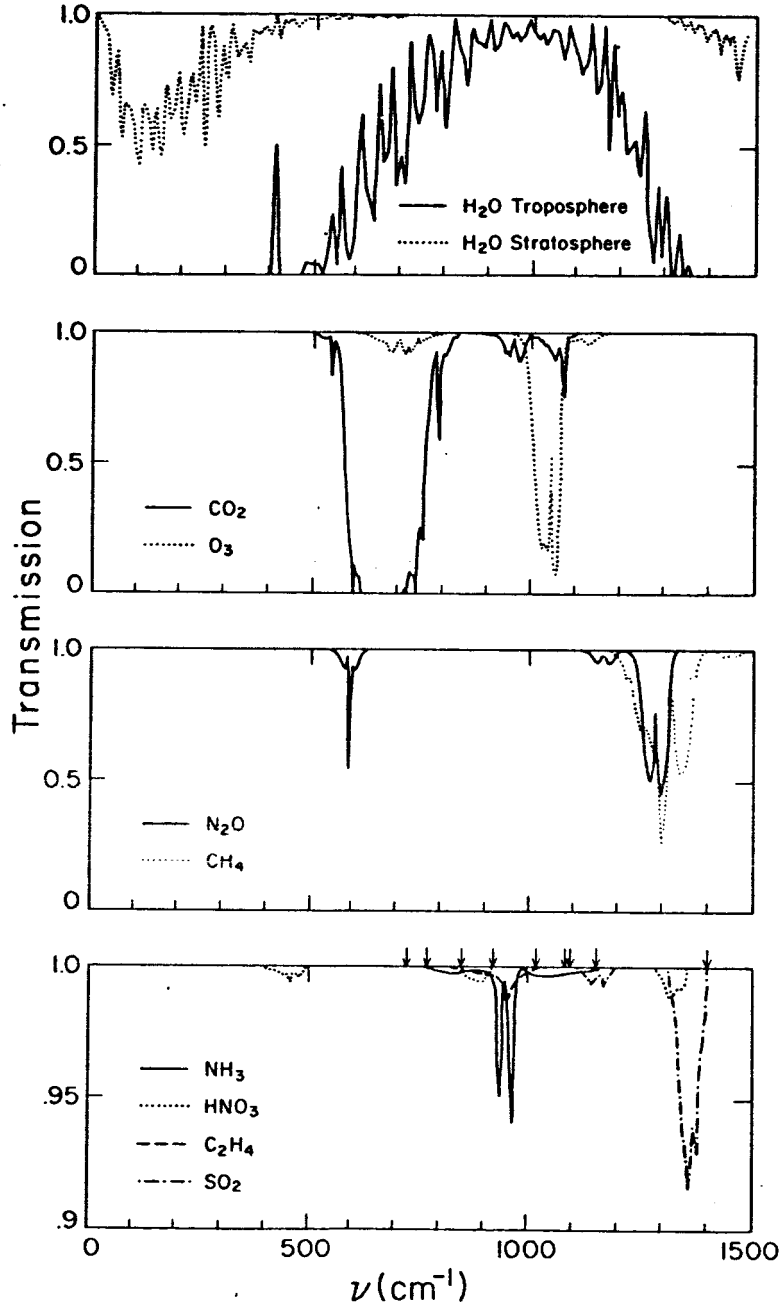
1.0
0.5
0
H_2O Troposphere
H_2O Stratosphere
CO_2
O_3
N_2O
CH_4
NH_3
HNO_3
C_2H_4
SO_2
.95
.9
Transmission
0
500
1000
1500
$\nu(cm^{-1})$

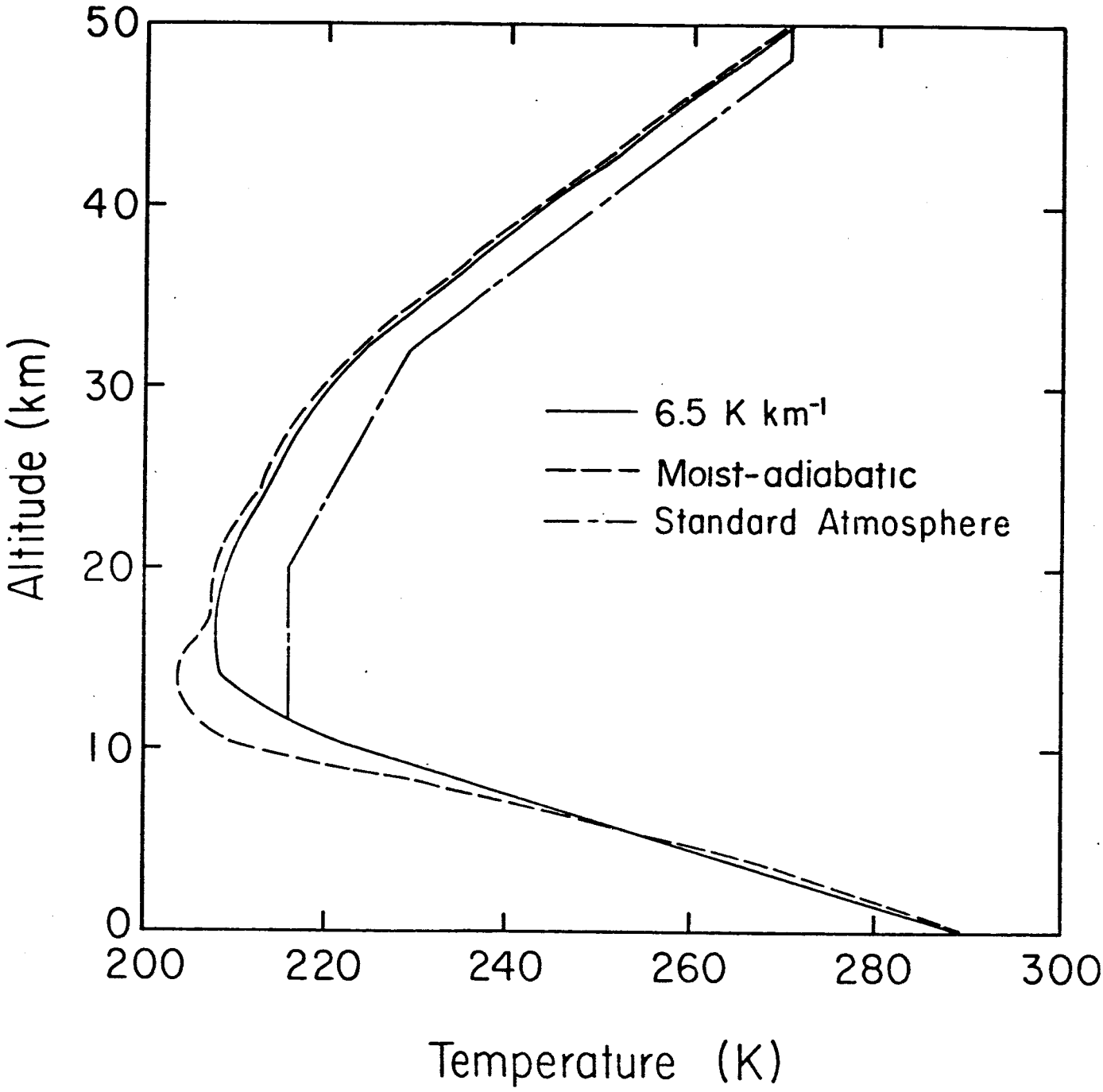
50
40
30
20
10
0
Altitude (km)
200
220
240
260
280
300
Temperature (K)
6.5 K km⁻¹
Moist-adiabatic
Standard Atmosphere

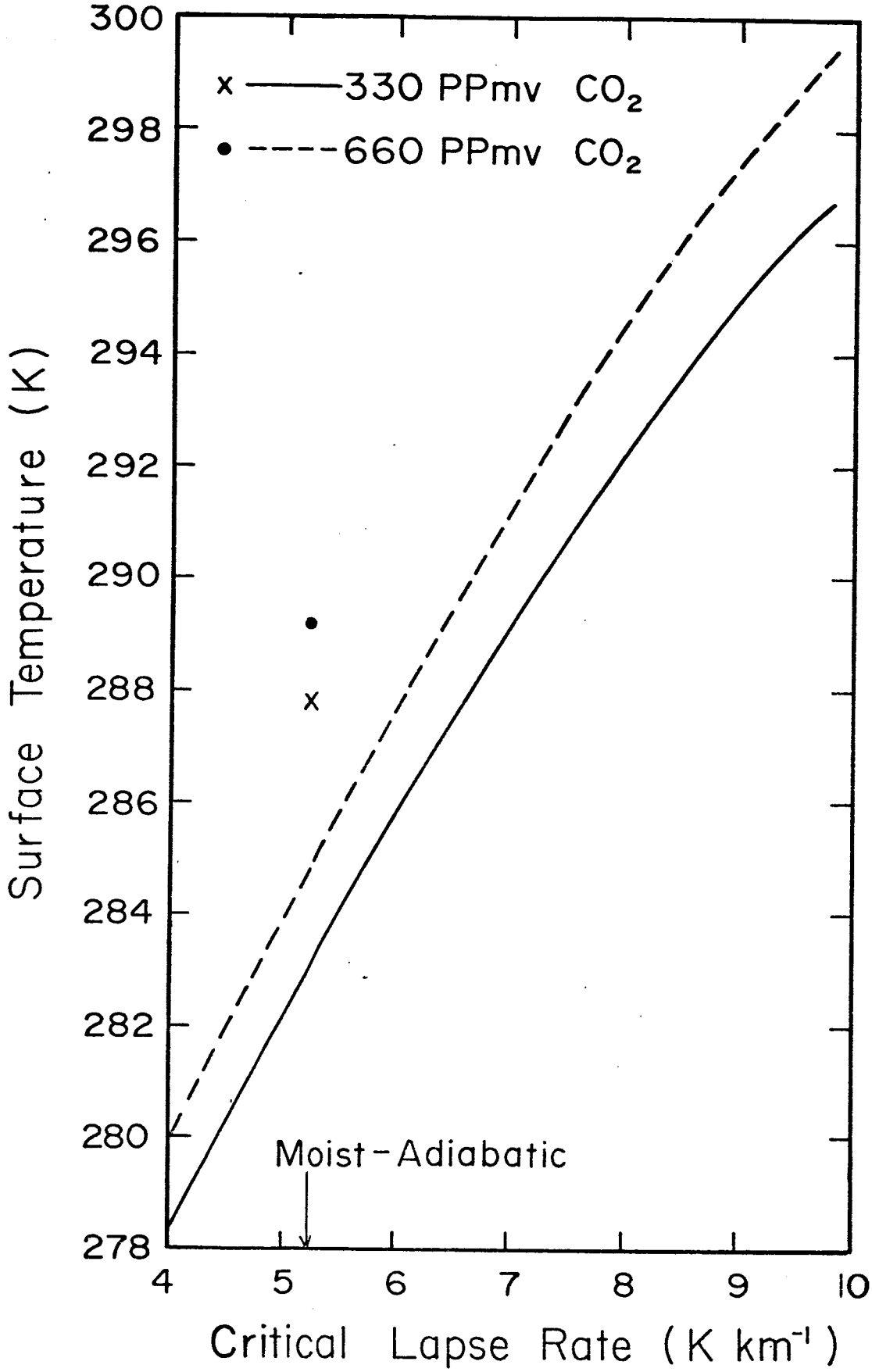
300
298
296
294
292
290
288
286
284
282
280
278
x ——330 PPmv CO_2
• ----660 PPmv CO_2
Surface Temperature (K)
Moist-Adiabatic
4
5
6
7
8
9
10
Critical Lapse Rate (K km^{-1})

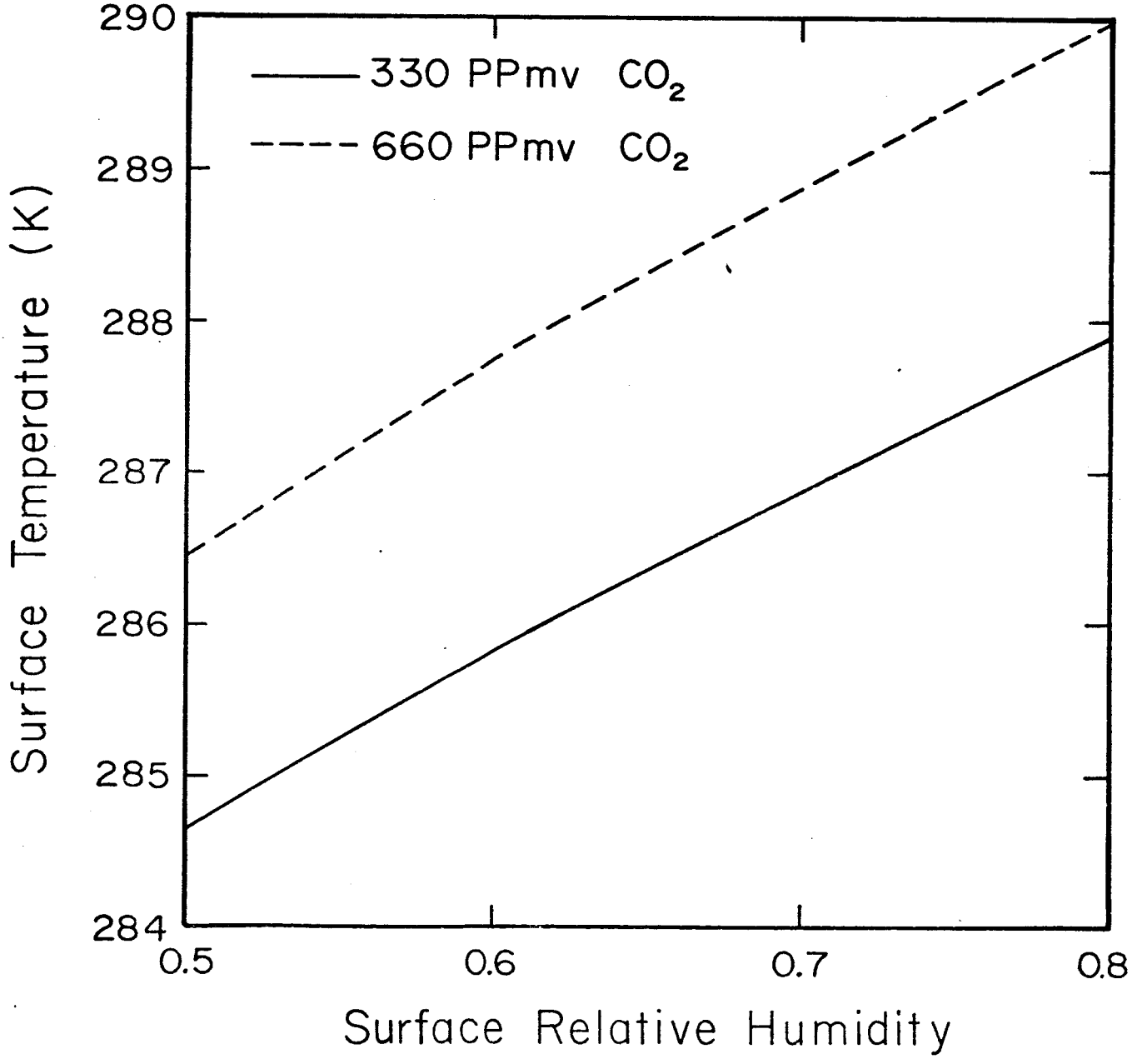
290
289
288
287
286
285
284
330 PPmv CO2
660 PPmv CO2
Surface Temperature (K)
0.5
0.6
0.7
0.8
Surface Relative Humidity

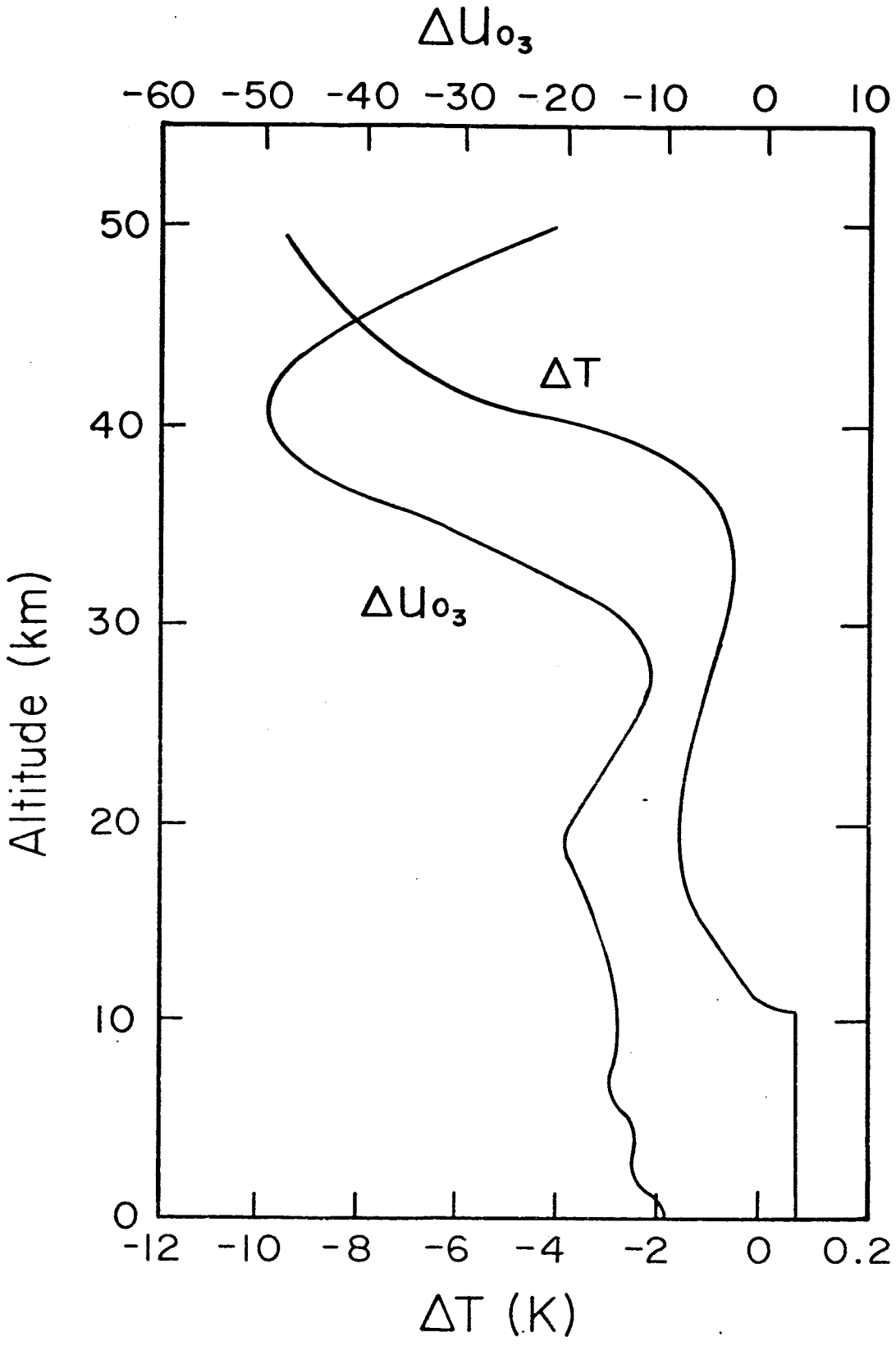
ΔU$_{O_3}$
-60 -50 -40 -30 -20 -10 0 10
50
40
30
20
10
0
ΔT
ΔU$_{O_3}$
Altitude (km)
-12 -10 -8 -6 -4 -2 0 0.2
ΔT (K)